

pubs.acs.org/ac Article

# Real-Time Investigation of Primary Ship Engine Emissions by Vacuum Resonance-Enhanced Multiphoton Ionization High-Resolution Orbitrap Mass Spectrometry

Paul Kösling, Christopher P. Rüger,\* Julian Schade, Sven Ehlert, Uwe Etzien, Anton N. Kozhinov, Yury O. Tsybin, Martin Rigler, Thomas Adam, Andreas Walte, Bert Buchholz, and Ralf Zimmermann



Cite This: Anal. Chem. 2022, 94, 16855-16863



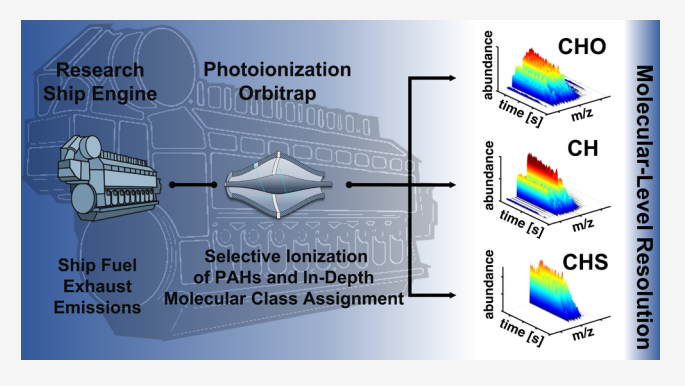
**ACCESS** I

III Metrics & More

Article Recommendations

Supporting Information

ABSTRACT: The comprehensive chemical description of air pollution is a prerequisite for understanding atmospheric transformation processes and effects on climate and environmental health. In this study, a prototype vacuum photoionization Orbitrap mass spectrometer was evaluated for field-suitability by an online on-site investigation of emissions from a ship diesel engine. Despite remote measurements in a challenging environment, the mass spectrometric performance could fully be exploited. Due to the high resolution and mass accuracy in combination with resonance-enhanced multiphoton ionization, the aromatic hydrocarbon profile could selectively and sensitively be analyzed. Limitations from commonly deployed time-of-flight platforms could be overcome, allowing to unraveling the oxygen- and sulfur-containing



compounds. Scan-by-scan evaluation of the online data revealed no shift in exact m/z, assignment statistics with root mean square error (RMSE) below 0.2 ppm, continuous high-resolution capabilities, and good isotopic profile matches. Emissions from three different feed fuels were investigated, namely, diesel, heavy fuel oil (HFO), and very low sulfur fuel oil (VLSFO). Regulations mainly concern the fuel sulfur content, and thus, exhaust gas treatment or new emerging fuels, such as the cycle-oil-based VLSFO, can legally be applied. Unfortunately, despite lower CHS-class emissions, a substantial amount of PAHs is emitted by the VLSFO with higher aromaticity compared to the HFO. Hence, legislative measures might need to take further chemical criteria into account.

## INTRODUCTION

Air pollution was found to significantly alter the atmospheric physicochemistry and cause a substantial burden to the globe through climate change. Aside, air pollution causes considerable environmental health effects. Therefore, a molecular-level description of the pollution sources is crucial for understanding their environmental fate and toxicological impact. Among emission sources, maritime transport logistics was shown to play an essential role. In 2015, more than 80% of the global transportation of goods was performed via the sea. The rising demand for shipping and the lack of international restrictions increased the relevance. Consequently, ship emissions have become one of the main contributors to air pollution.

Shipping emissions exhibit a unique molecular profile, <sup>5–7</sup> different from other sources, such as biomass burning <sup>8</sup> or onroad engine emissions. <sup>9,10</sup> Historically, bunker fuels, a heavy residue of fossil petroleum refining with a high sulfur content and rich in aromatic constituents, have been used due to market availability and low prices. In this context, reduction measures have been introduced to limit emissions, such as sulfur emission control areas (SECAs) in epicontinental seas.

Here, fuel-sulfur content (FSC) has been limited to 0.1% (m/m) since 2015. In 2020, a novel regulation limiting the FSC from 3.5 to 0.5% (m/m) by the International Marine Organization (IMO) became effective internationally. Consequently, these regulations lead to an overall broadening in the market, adapted shipping fuel landscape, and emerging novel fuel compositions. The modest analytical procedures given in ISO 8217 do only specify the propellants, not their exhaust gases. Even so, the sulfur content is regulated, for example, to reduce  $SO_x$  emissions, the specification for gaseous compounds is very limited. Nonetheless, due to the high complexity and challenging molecular profile of ship emissions, it is necessary to use various systems that allow us to comprehensively understand the organic matrix. In this regard,

Received: September 9, 2022 Accepted: November 11, 2022 Published: November 23, 2022





state-of-the-art instrumentation like the aerosol mass spectrometer (AMS), 11,12 extractive electrospray ionization (EESI), <sup>13</sup> or aerosol time-of-flight (ToF)<sup>14–16</sup> mass spectrometer have shown tremendous potential. Nevertheless, these advanced approaches are targeting the particle phase of the aerosol. Complementarily, it was shown that the in-depth description of the gas phase is of equal importance. Commonly, gaseous compounds can be trapped and sampled on cartridges for subsequent laboratory analysis, for example, for profiling the carbonyls. 18,19 Despite high sensitivity and selectivity, the time-dependent information is often lost. Online mass spectrometric profiling often relies on lowerresolving time-of-flight mass spectrometry platforms, making it harder to identify species in the complex matrix with high confidence. Nonetheless, it was shown that these ToF systems could investigate dynamical processes from various emission sources. 20-23 Laser-based resonance-enhanced multiphoton ionization (REMPI) is frequently deployed, focusing the analyses on polycyclic aromatic hydrocarbons (PAHs), which are known for their mutagenic/carcinogenic health effects. Particularly, primary engine emissions have shown high contributions of PAHs, for ship emissions largely resulting from unburned and partially burned feed fuel. More importantly, due to the high content of heteroatoms (nitrogen, sulfur, oxygen, and metals) in the feed fuel, ship emissions contain not only core or alkylated PAH species but also nitrogen- and sulfur-containing derivatives (PASH/N-PAHs) as well as oxidized components (oxy-PAHs). Discovering this molecular complexity requires high-resolution performance of mass spectrometers due to the mass spectral overlaps with other compounds. Therefore, molecular-level monitoring with improved differentiation of PAHs, PASHs, N-PAHs, and oxy-PAHs of ship emission sources is of high interest<sup>24</sup> and lacks suitable robust field instrumentation.

We investigate the primary emissions of a marine ship diesel engine by a novel vacuum photoionization (REMPI) highresolution mass spectrometer. For this purpose, a field campaign at an engine facility studying a four-stroke singlecylinder research engine operated with different feed fuels (diesel, very low sulfur fuel oil (VLSFO), heavy fuel oil (HFO)) was realized. These complex fossil petrochemical feed fuels result in complex emissions acting as an ambitious testbed for the state-of-the-art Orbitrap analyzer-equipped platform. Our recently introduced modified Exactive Orbitrap (PhotOrbi) deployed with vacuum REMPI is evaluated here.<sup>25</sup> The high resolution, spectral dynamic range, and mass accuracy of the Orbitrap platform are used to explore not only PAHs but also PASHs, N-PAHs, and oxy-PAHs. These compounds have been previously "hidden" from most online mass spectrometric approaches. This study aims to demonstrate the field applicability of the robust PhotOrbi system for on-site profiling of complex emission profiles in a challenging high-temperature and vibrating environment.

## MATERIALS AND METHODS

Ship Diesel Engine Field Campaign. In this study, the primary ship diesel emissions of three different feed fuels, namely, marine gas oil (Diesel, FSC < 0.1 wt %), heavy fuel oil (HFO, FSC 1.7 wt %), and very low sulfur fuel oil (VLSFO, FSC 0.5 wt %), were investigated. For this purpose, the fuels have been fed to a four-stroke single-cylinder research diesel engine (75%/60 kW cruise state and 25%/20 kW harbor maneuvering engine load, displacement: 3,2 l). Additionally, to

address novel IMO regulations, measurements were performed with HFO as a feed and a wet exhaust treatment system (scrubber).

Experimental Setup and Sampling. The vacuum photoionization Orbitrap (PhotOrbi) was installed in a room directly next to the research ship diesel engine. A photograph and scheme of the simplified experimental setup are given in the supporting information (Figure S1). The instrument was coupled to the engine exhaust tubing at two connection points. The first one is sampling directly after the engine, resulting in high exhaust gas temperatures between 300 and 400 °C, whereas the second point is located after the scrubber exhaust treatment. For the latter, a significantly lower exhaust gas temperature of about 30 °C has been found. The raw exhaust gas, a mixture of particle and gaseous phase, was filtered with a heated filter unit (250 °C, stainless-steel holder with a candle filter F-0, 1GF, M&C Tech Group, Germany). The connection between the sampling point and filter unit to the exhaust gas pipe was realized by a 5 m stainless-steel tube and a heated transfer line operated at 250 °C. A modified gas chromatography oven was used to uniformly heat the filter unit as well as the sample tubing and dilution to prevent saturation and contamination of the mass spectrometer. The exhaust gas concentration was regulated and diluted by a flow-controlleradjusted nitrogen supply (≥99.999 v %) prior to the heated filter unit. Adapting this initial dilution flow and the flow after the PhotOrbi inlet (waste split) allowed to regulate the overall sampled exhaust gas and dilution. By adjusting the nitrogen flow due to the implementation of a flow controller before the filter and a second flow controller between the connection to the PhotOrbi and the membrane pump, the incoming exhaust gas flow could be regulated. For the measurements, at sampling point one, a dilution ratio of 1:5 was used. At the second sampling point (30 °C), less concentrated gas was measured; thus, no further dilution was necessary. Following the heated filter and dilution setup, the PhotOrbi is connected by a heated, deactivated fused-silica capillary (ID: 250  $\mu$ m, length: 9 m, 250 °C). The diluted primary exhaust emissions are introduced in the mass spectrometer unit by a heated inlet, consisting of a heated capillary oven and a heated brass tip (both at 250 °C). Compared to the recently introduced PhotOrbi platform, this is a revised version with fewer coldspots and improved sample transfer also for higher molecular weight compounds.<sup>25</sup> The injected gas mixture is ionized by a (1 + 1) REMPI process inside of the C-trap of the Orbitrap assembly utilizing a KrF excimer laser at a wavelength of 248 nm and a laser energy of 192 µJ. Mass spectra were generally acquired with a resolution setting  $R = 140\,000$  at m/z200, which refers to an acquisition speed of about 2 Hz. The phased time-domain transients were acquired in parallel with mass spectra via the external high-performance data acquisition system (FTMS Booster X2, Spectroswiss, Lausanne, Switzerland), as described elsewhere. 25 System performance has been evaluated daily by measuring a standard gas mixture (Figure

**Data Evaluation.** An extensive description of the mass spectrometric data collection and processing is given elsewhere. In brief, the pre-processing of the recorded data is done by Peak-by-Peak Base Edition software suite (version 2022.7.0, Spectroswiss), which includes conversion of the phased time-domain transients into the mass spectra represented in the absorption mode (aFT). The post-processing is realized by two methods, first by a scan-by-scan

evaluation of the collected mass spectral information and second by time-domain transient averaging over certain time intervals/processes with stable conditions (same feed fuel and load settings). The attribution of the elemental compositions is done by a custom MATLAB (MATLAB R2020b) graphical user interface using the following boundaries: error width 1 ppm (scan-by-scan processing), 2 ppm (time-segment averaged processing); elemental composition restrictions  $C_{1-100}H_{1-200}N_{0-1}O_{0-2}S_{0-1}$ , DBE range: 0–30, mass range: 50–500 Da.

#### RESULTS AND DISCUSSION

Studying Ship Diesel Engine Emissions-Robustness and Field Versatility. In this study, the recently introduced photoionization Orbitrap mass spectrometer was tested and evaluated for the first time for its field suit and applicability. For this purpose, the figures of merit of the high-resolution mass spectrometric unit performance as well as the ionization characteristics are discussed in the following. This procedure is crucial to observe the instrumental parameters under nonideal, nonlaboratory, remote conditions, affected by thermal instability, changing humidity, vibrations, and transport. Survey visualization of the time-resolved mass spectrometric information is generally used in ToF mass spectrometric approaches<sup>23</sup> and allows for a first molecular insight into the overall emission characteristics. Exemplarily, Figure 1 displays the daily starting behavior of the ship diesel engine; the changes in the molecular profile can easily be traced.

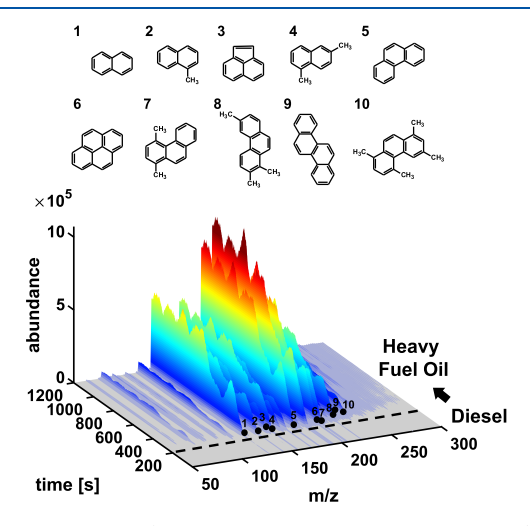
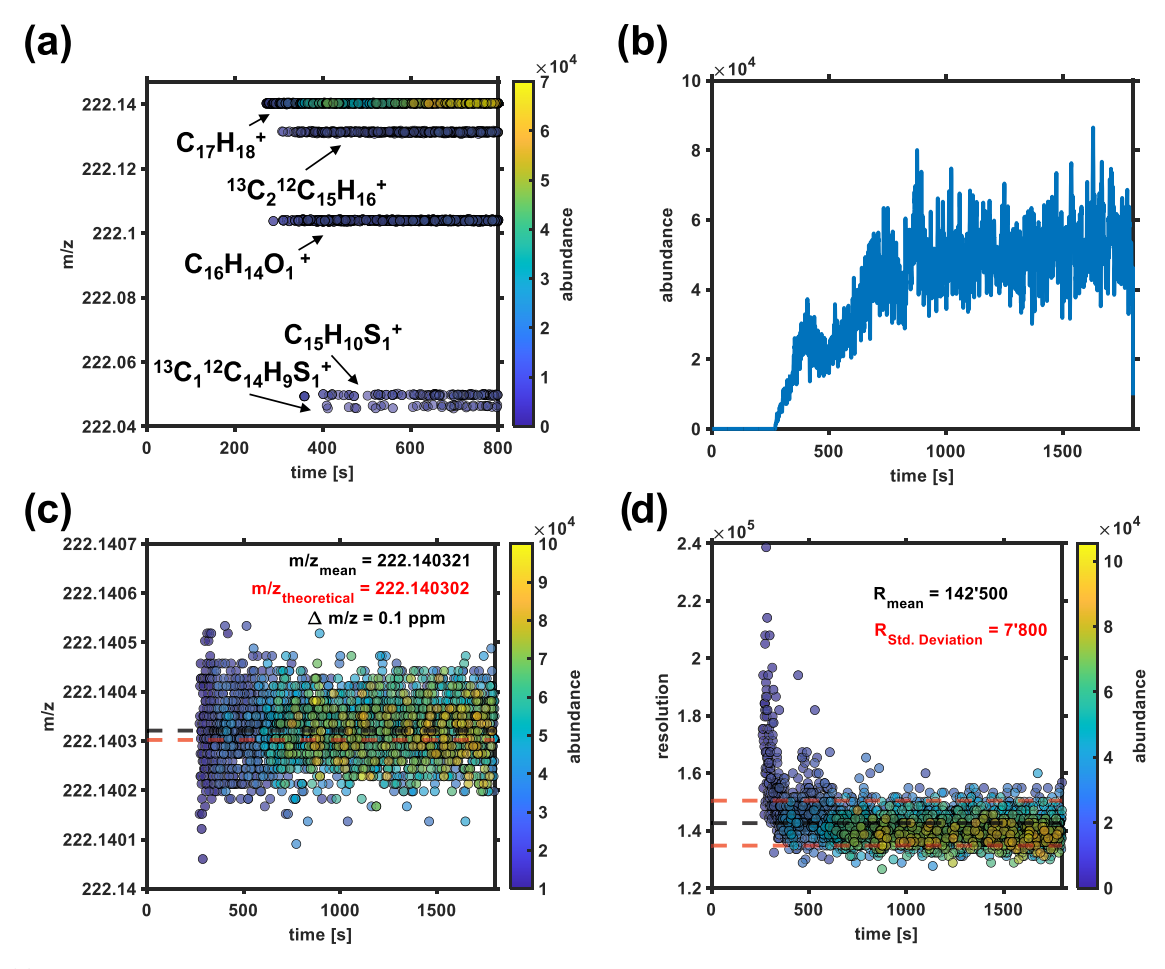


Figure 1. Survey plot (m/z versus time, abundance color-coded) of an exemplary engine launch. From start to approximately 200 s, the engine is operated with distillate diesel fuel. The change to a residual bunker fuel (heavy fuel oil, HFO) leads to an enormous increase in abundance and molecular complexity, traced online via the photoionization high-resolution mass spectrometer (PhotOrbi) at about 2 Hz acquisition rate. Ten traces are marked exemplarily, and tentative chemical structures are given.

More in detail, the research engine was launched and operated with clean diesel fuel (DIN EN 590) for several minutes. After this heating-up phase, the fuel type was switched to either HFO or VLSFO. In this example, the changes in the primary exhaust emissions for the switch from diesel to HFO are depicted, both at a nominal load of 20 kW. The photoionization high-resolution mass spectra recorded during the starting phase (<200 s), resulting from the

combustion of diesel fuel, only featured low abundances of polycyclic aromatic hydrocarbons without alkylation (so-called "core" structures) up to an m/z of 228, for example, chrysene. It has to be highlighted that the deployed REMPI scheme solely ionizes aromatic constituents, whereas nonaromatic compounds within the primary diesel emission, such as alkanes, alkenes, or aldehydes, are not accessed.<sup>25</sup> Consequently, an overall minimal number of compounds (average 0-200 s, n = 202) has been identified, specifically the pyrogenic-formed PAH cores, with  $C_{16}H_{10}$  (m/z 202) being the dominant ones. Online ToF photoionization MS has been previously reported on these compounds within a range of lowv-ppb traces up to v-ppm,<sup>26</sup> and the here evaluated PhotOrbi platform is capable to detect them. Furthermore, unique molecular formula attribution below 1 ppm has been achieved despite the low signal-to-noise ratio (Figure S3). During the transition phase from the distillate fuel diesel to the bunker HFO feed (200-800 s), the mass spectrometric complexity drastically increases with broader coverage in m/z and isobaric diversity, with a maximum of up to six signals per nominal mass. Moreover, the total ion current (TIC, Figure S4), as well as the abundances of the entirety of the individual signals (extracted ion currents, EICs), significantly increased by several orders of magnitude. Aside from core PAHs, formed primarily pyrogenically, alkylated PAHs and polycyclic aromatic sulfur heterocycles (PASH) dominate the mass spectra. These compounds can classically be related to a high contribution of unburned fuel, 27,28 reported for ship diesel engines fed with bunker fuels. Even though for PASH (which behaves similarly to halogenated PAHs<sup>29,30</sup> due to the heavy atom effect) low ionization cross-sections have been reported, due to the short lifetime of the excited transition state in the REMPI process, high concentrations in the primary ship diesel emissions of the bunker fuels with sulfur fuel content above 0.5 wt % cause a substantial mass spectrometric response. Aside, also more polar constituents, such as oxygen-containing compounds, for example, oxy-PAHs, are detected as a product of incomplete combustion.<sup>31</sup> These polar compounds can directly and confidentially be differentiated from other constituents and are of high interest with respect to environmental aging and alteration of the emissions as well as toxicological effects. 32,33 In routinely deployed ToF platforms, these CHO-class species might be analytically hidden below strong contributions of the alkylated CH-class series and its isotopic fingerprints.

Given the highly dynamic processes and enormous differences in engine emission and pattern, the launching phase and transition from a distillate to residual feed fuel act as an ideal case for the Orbitrap high-resolution mass spectrometric figures of merit, such as resolution, mass accuracy, stability, and inter-spectral abundance spread, discussed in the following. For the Fourier transform (FT) mass analyzer, being a class of ion traps, controlling and limiting the number of injected ions (charges) is crucial for maintaining high performance. Consequently, in this first field deployment of the PhotOrbi platform, a conservatively high dilution of the primary exhaust gas and a single-laser-shot ionization event per mass spectral recording should avoid overfilling of the C-trap and Orbitrap, respectively. Thus, even though not having automatic gain control (AGC) capabilities, initially provided by commercial atmospheric pressure Orbitrap mass spectrometers to regulate the number of injected charges, overfilling and space charge effects are safely minimized. Nonetheless, as a drawback, the



**Figure 2.** (a) Time-resolved visualization of the isobaric complexity at m/z 222, color-coded according to abundance. The isobaric interferences can be entirely resolved. (b) Extracted ion chromatogram (EIC) of  $C_{17}H_{18}^+$  revealing the appearance during the change from diesel to heavy fuel oil and stabilization after approx 1000 s. (c) Time-resolved scatter plot of the exact m/z position, color-coded according to EIC abundance. The mean value is marked with a dashed black line, whereas the theoretical value is given as a red dashed line ( $\Delta m/z$  0.1 ppm). (d) Time-resolved scatter plot of the resolution of the  $C_{17}H_{18}^+$  signal, color-coded according to EIC abundance. Lower ion currents, in the beginning, cause an improved resolution with a later stabilization. Histograms of the data from (c, d) are given in Figure S5.

dynamic range of the Orbitrap analyzer is not fully exploited and ratios of roughly 1e2 (100–280) between single-scan highest and lowest abundant peak-picked signal (noise thresholding factor of one, which corresponds to about five standard deviations of noise) can be determined (Figure S6a). Despite being one order of magnitude lower than the classically reported ranges, this value has been found to be very stable and highly reproducible, given a stabilization of the ion load and emission source. Figure 2a displays the time-resolved insight into the isobaric complexity of nominal mass m/z 222. Here, the analytical benefit of separating and identifying the aerosol compounds can be seen immediately.

Aside from the most dominant trace,  $C_{17}H_{18}^{\bullet+}$ , the radical cation of presumably a  $C_4$ -alkylated fluorene or  $C_3$ -alkylated dihydroanthracene (double bond equivalence, DBE, of 9), traces of CHS and CHO as well as  $^{13}$ C isotopologues of CH-class compounds can be identified. With nominal resolution, these traces would remain hidden, and solely, the dominant PAH compound would have been identified. Moreover, attribution heavily relies on literature work on comparable emission sources, utilizing offline sampling and in-depth labbased characterization, such as gas chromatography coupled with MS(GC-MS). Despite not directly extracting isomeric information, accurate mass information by high-resolution MS

enables an added additional validation dimension, even if there would have been only one trace per nominal mass. Despite sudden occurrence and steady increase in abundance till the steady state at roughly 1000 s, no shifts or distortions of the locations of the m/z traces can be found. This m/z stability and accuracy can even be better depicted in Figure 2b,c,e, combining scan-resolved expanded view of the m/z trace of  $C_{17}H_{18}^{\bullet+}$  (m/z 222.1403), the respective EIC as well as histogram distribution of the exact peak-picked positions. Alkylated fluorene derivatives are common petrogenicresiduals from the feed fuel and, thus, occur at the switch from clean distillate diesel fuel to heavier HFO. Nonetheless, the exact m/z position is not shifting and is centered with a symmetric Gaussian distribution with a full width at half maximum (FWHM) of below 0.4 ppm. The mass deviation of the mean value to the theoretical value after recalibration is below 0.1 ppm. For the entire broadband molecular complexity, the error distribution for the molecular formula attribution can be found in Figure S3 with a root mean square error (RMSE) of 0.18 ppm for approx. 400 attributed signals.

The robustness of the high mass resolving power delivered by the FT Orbitrap mass analyzer is crucial. Figure 2d,f exemplarily displays the time-resolved FWHM resolution of the already discussed  $C_{17}H_{18}^{\bullet+}$  (m/z 222.1403) signal over a

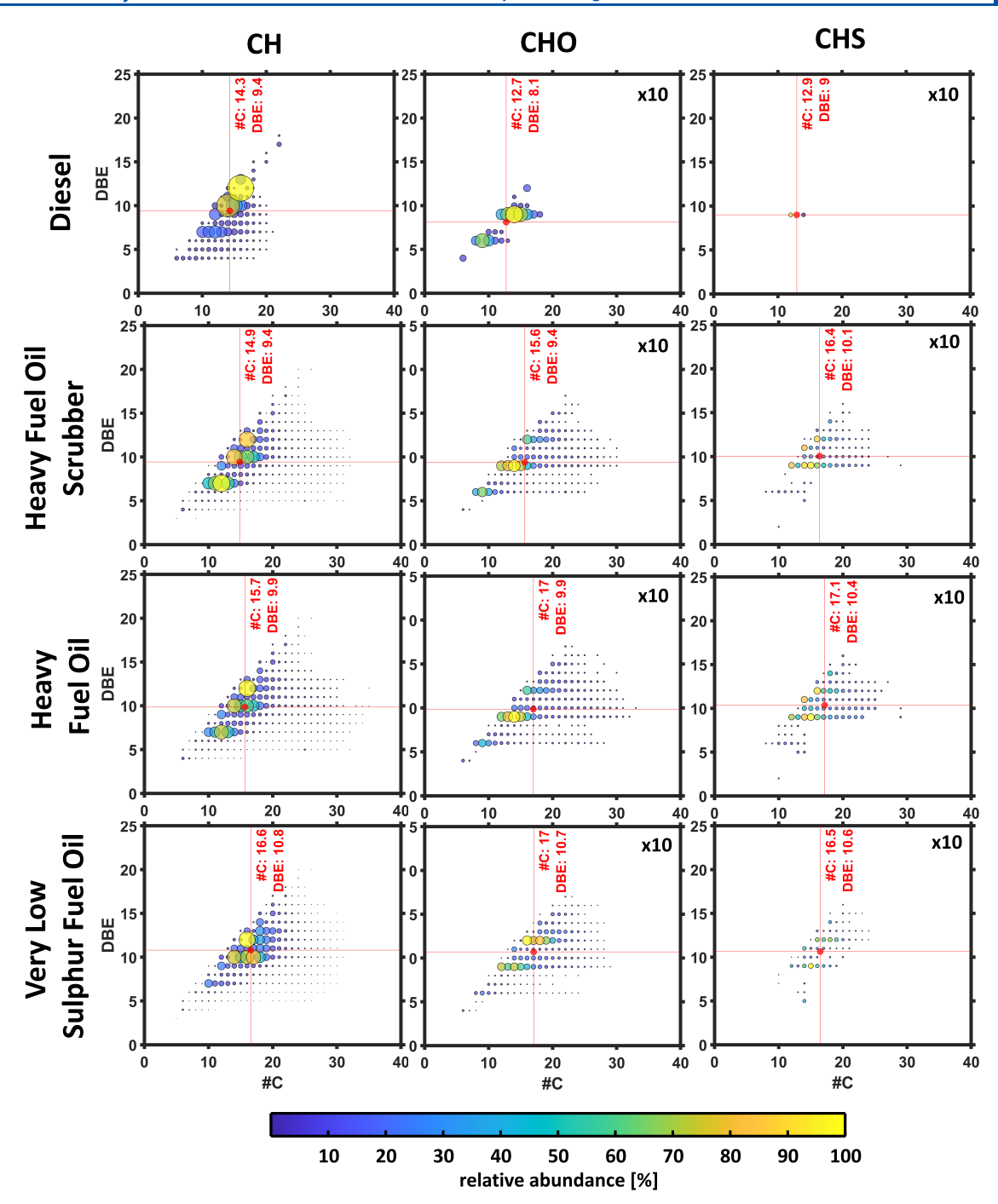


Figure 3. Carbon number versus DBE visualization of the CH-, CHO-, and CHS-class for the primary exhaust gas emissions of various feed fuels (diesel, heavy fuel oil—HFO, very low sulfur fuel oil—VLSFO). HFO emissions after the scrubber exhaust gas treatment are given for completion. The displayed data are average chemical speciation from 5 min of stable 20 kW load emissions. Data are color-coded according to the relative abundance within the respective sample and compound class. Abundance-weighted mean carbon number and DBE values are given in red.

time interval of over 1000 s. As for the m/z position, a stable and robust behavior of the FWHM can be found. Resolution is within the specification for a low-field D30 Exactive-series orbitrap mass analyzer operated in absorption mode. A symmetric Gaussian distribution of the m/z FWHM with a resolution of over 140 000 at m/z 200 is registered. Most importantly, the resolution is not negatively affected by the abundance of the individual signal or the overall number of charges (TIC) with an FWHM of the distribution below 10%. Interestingly, for very low TIC and EIC values (appearing below 500 s), an even improved higher resolution can be

observed. Common mass splits, such as  $^{12}\text{C}^1\text{H}_4$  versus  $^{16}\text{O}$  ( $\sim 36.4$  mDa) and  $^{12}\text{C}_3$  versus  $^{32}\text{S}^1\text{H}_4$  ( $\sim 3.4$  mDa), can be seen in Figure 2a and are fully or sufficiently (at higher m/z) resolved for peak picking within the observed analytical m/z range of 50–300 Da. Comparing with other mass analyzers, such as ToF platforms, a resolution of at least 60 000–80 000 is required at m/z 350 (upper end of the here-found emission pattern) for reliable differentiation of these mass splits; parameters have only recently been achieved by quadrupole orthogonal-acceleration ToF systems and not reported in a comparable field-study usage.

For evaluation of the isotopic fine structure pattern, particularly, simulations of isotopic distributions can be helpful, conducted in this work via the FTMS Simulator software tool (Spectroswiss). Figure S6b compares the theoretical and experimental isotopic distribution of C<sub>16</sub>H<sub>10</sub><sup>•+</sup> (m/z 202.0777) for the averaged spectrometric information. Generally, deviations are below 10% (theoretical versus the experimental abundance of a <sup>13</sup>C isotopologue relative to the abundance of this isotopologue) (Figure S8). This performance is achieved over several thousands of scans during the online emission measurement (Figures S6 and S7) without trend and standard deviation below 2-3% (relative to the monoisotopic signal). Consequently, the high-resolution MS PhotOrbi platform can harvest not only the exact mass positions of the monoisotopic signals and their respective isotopologues but also an isotope-based exclusion of impossible attributions as additional validation. Notably, the response of CHS-class compounds has been too weak for an evaluation of the sulfur isotopes (32S 95.02% versus 34S 4.21%).

The applied REMPI process leads to an efficient and selective ionization of unsaturated constituents.<sup>34</sup> A detailed discussion on the ionization characteristics can be found in the supporting material (Figure S9). Briefly, REMPI is selectively exploiting the aromatic portion of the chemical space as a crucial fraction with respect to unburned/partially burned fuel (petrogenic) and/or the formation of combustion products and soot precursory (pyrogenic).

Application toward Feed Fuel Emission Characteristics. In the following, a comparison of the deployed feed fuels is discussed. For this purpose, a 5 min response of stabilized engine emissions is summarized and elemental composition is attributed. For visualization of the complex mass spectrometric data (Figure S10), commonly so-called fingerprint plots, such as the carbon number (#C) versus DBE (measure for hydrogen deficiency, that is, unsaturation/ aromaticity), are used. Figure 4 displays the #C versus DBE molecular maps ([M]+•) for the feed fuels (diesel, HFO, and very low sulfur fuel oil) for the CH- and CHO-class. Data for the HFO emissions are given with and without the usage of a wet scrubber for exhaust gas treatment. Despite the softness of the vacuum photoionization, highly alkylated constituents are prone to a certain degree of fragmentation, for example, causing a continuous signal of  $C_{15}H_9$  at m/z 189. These processes generally result in even-electron configuration ([M+  $H^{+}/[M-H]^{-}$ ). The overall abundance of these artifacts is low and in the single-digit percentage. Beneficially, the capabilities of the high-resolution mass analyzer allow for a separation of the even and odd electron-configuration signals, discussing the intact species solely. It has to be assumed that this general ionization effect was similar in previous studies, but due to the usage of limited ToF technology not differentiable from the intact molecular pattern or <sup>13</sup>C isotopologues.

As expected, the distillate diesel fuel shows the least complex emission pattern with a low degree of alkylation (horizontal lines) and a maximum carbon number of 22. In contrast, the HFO and VLSFO primary emissions exhibit a significantly higher complexity with broader coverage of the molecular space, reaching up to carbon number 32. The same observation can be made for the DBE, where for the diesel emissions values above 12 are only rarely found and a strong population can be found for the nondistillate fuels HFO and VLSFO. Interestingly, for the CHO-class, the diesel emissions

only reveal a very low number of core-structural motives (DBE series) with a maximum of 5-6 in alkylation length. Here, specifically, the oxygen-containing alkylated PAH series of benzo- and dibenzofuran (DBE 6 and 9) can tentatively be attributed. Concerning the environmental fate or direct toxicological impact on humankind, these more polar constituents can be more easily absorbed via the respiratory system and might cause other metabolomics pathways compared to CH-class PAHs.<sup>35</sup> Moreover, homologous series of classical oxidation products of the PAHs, forming oxy-PAHs at DBE 7 or 10, have only slightly been observed for the primary diesel emissions. For the HFO and VLSFO emissions also, the CH-class compounds are the most dominant, but generally, longer alkylation pattern can be found. Interestingly, the VLSFO exhibits increased abundances for higher DBE values compared to the HFO with DBE 12, for example, pyrene/fluoranthene, being a dominant series, despite significantly lower FSC of the VLSFO. Hence, regardless of being considered as cleaner feed fuel in the shipping industry, as given by the molecular observation, combustion of the VLSFO will cause a substantial release of larger PAHs with a potentially higher carcinogenic impact on environmental health. This phenomenon is also given for CHO-class, which for both, HFO and VLSFO, is considerably more complex than the diesel emission CHO-class. Here, also oxygenated analogoues of the EPA PAHs, such as oxy-pyrene (DBE 12), can be attributed. The high content of aromatic constituents, despite a low FSC, was previously validated by comprehensive gas chromatography and thermal analysis mass spectrometry investigating various bunker fuels and a comparable VLSFO.<sup>3</sup>

The molecular diversity of the PASH class is given in Figure 3. In agreement with the very low FSC of the diesel fuel of below 0.1 wt %, specified by the DIN EN 590 norm, only three signals at DBE 9 with a relative abundance of 0.18% could be found. These species could also be caused by residues and carryover from past usage of the ship diesel engine or from the lubrication oil. The VLSFO exhibits a simple distribution, centered at DBE of 10-11, for example, between dibenzo-(DBE 9) and benzonaptho-thiophenic (DBE 12) structures, spreading #C 9-24 and DBE 5-16, with a relative abundance of 1% for the CHS-class. For the HFO, the broadest CHS-class pattern with the highest number of attributed signals is found with a relative abundance of 3.3%. Here, the homologous series of DBE 9, 11, and 12, are dominant, and even DBE 15 series, for example, dinaptho-thiophens, can be observed. Interestingly, the relative abundance of the CHS-class for the three feed fuels being 0.18, 1, and 3.3% for the diesel, VLSFO, and HFO, correlates with the FSC of <0.1, 0.5, and 1.7 wt %, respectively. We hypothesize that this behavior is partially caused by the ionization cross-sections being dominantly determined by the aromatic core structure with low contribution from the alkylation side chains. Hence, as for the petroleum-feed fuels, similar thiophenic aromatic motifs can be expected, intercomparison of feed fuel results is feasible.

The effect of the wet-scrubber exhaust gas treatment on the sampled emission and targeted molecular profile is very low and almost negligible. CH- and CHO-class plots (Figure 3) are practically identical. Solely, a very low impact on the upper carbon number limit (alkylation length) can be concluded based on a shift in the observed upper mass limit. Taking into consideration the residence time of a few seconds within the scrubber unit as well as the design for  $SO_x$  removal, this finding is not unexpected. Nonetheless, in the context of hazardous

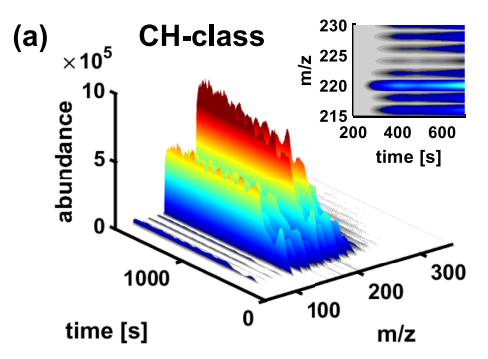
emissions by ship diesel engines, legal freighting with HFO and the deployed scrubber unit will result in a substantial and almost identical PAH emission pattern. Considering the high impact of PAHs on environmental health, further emission reduction and treatment actions should be considered by lawmakers,<sup>37</sup> based on unraveling the molecular diversity by the PhotOrbi platform. Due to different sampling locations within the exhaust gas system and, thus, difficulties in adjusting the same dilution settings, no statements on the concentrations can be taken from this testing campaign data. Data reduction can be made by calculating the abundance-weighted mean carbon number and DBE value ("center of gravity"), given in red in Figure 3. Immediately, the main differentiation points, such as lower average #C for the diesel emissions and the highest average DBE for the VLSFO, can be depicted. Combined with the at-line data processing and elemental composition attribution feature of the PhotOrbi, this bulk information, based on the molecularly-resolved chemical pattern, might rapidly be used for emission characterization and classification, for example, utilizing the Kendrick mass defect plot for an entire class overview (Figure S15).

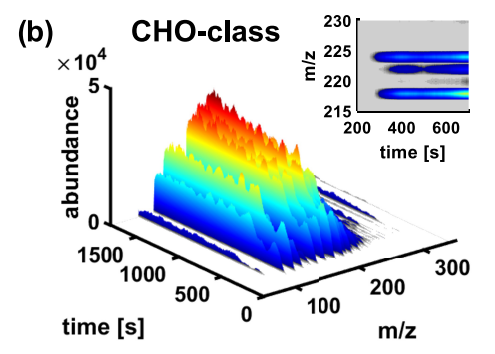
The online capabilities with >1 Hz time resolution are discussed from an applicative scenario, comparing the switch from diesel fuel to HFO or VLSFO. Figure \$16 exemplarily summarizes the extracted traces for the CH- and CHO-class, being the dominant compound classes (Figures S11-S14), as well as for  $C_{16}H_{10}O_1$  (DBE 10) and  $C_{15}H_{10}S_1$  (DBE 11). Notably, for both transitions, the abundance of all traces substantially increases after switching from the distillate clean diesel fuel to heavier feed fuel. In agreement with the FSC, both traces for C<sub>15</sub>H<sub>10</sub>S<sub>1</sub> are only occurring after the feed fuel change. The PhotOrbi platform allows to trace the stabilization behavior and fluctuation of the primary emissions on the total ion count level but, more interestingly, also for selected compound classes, directly calculated at-line from the elemental composition attribution or for individually resolved signals. Interestingly,  $C_{15}H_{10}S_1$  can be found for both cases with comparable abundance. The signal can tentatively be attributed to a methylated derivative of unsaturated thiophene derivatives, such as 3-methylphenanthro[4,5-bcd]thiophene or 8-methylacenaphtho[1,2-*b*]thiophene.

Figure 4 gives the survey plots (m/z) versus time, abundance color-coded) of the engine launch shown in Figure 1 (transition from diesel to heavy fuel oil). Here, the elemental composition attributions, enabled by the performance of the FT mass analyzer, allowed a back-calculation of the survey profiles, selectively visualizing the CH-, CHO-, and CHS-class compounds. Different molecular profiles can be depicted, particularly from the inset enlargements. Hence, despite the dominance of the CH-class with one to two orders of magnitude higher abundances, these heteroatom classes can directly be made visible online at the emission site. For common lower-resolving time-of-flight platforms, this information would be overlaid by the CH-class. However, TOF systems are able to trace faster processes up to 2000 Hz.<sup>38</sup> These heteroatom-containing compound classes are of high interest in environmental health studies and for correlations to a biological response. 39,40

# CONCLUSIONS

In this study, we successfully evaluated a vacuum photoionization high-resolution mass spectrometry platform (PhotOrbi) for the direct field usage in a remote nonlaboratory





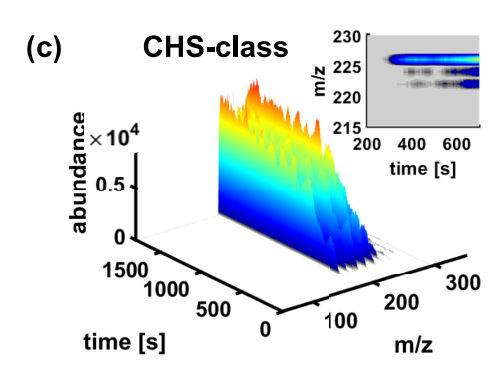


**Figure 4.** Survey plots (m/z) versus time, abundance color-coded) of the engine launch shown in Figure 1 (diesel  $\rightarrow$  heavy fuel oil) back-calculated based on the elemental composition attribution to (a) CH-class, (b) CHO-class, and (c) CHS-class compounds. Zoom into the molecular profile (m/z) 215–230 is given as 2D insets.

environment. The system was applied to study the primary combustion emissions of a research ship diesel engine online in the immediate vicinity. Despite transportation, fluctuation in surrounding temperature, and vibrations, the high performance of the Orbitrap mass analyzer combined with selective and sensitive REMPI could be maintained. More specifically, scanresolved processing of the mass spectrometric data revealed high resolution  $(m/\Delta m)$  above 140 000 at m/z 200, a high mass accuracy with negligible mass shifts and low ppm deviations.

Applied to the emissions of the ship diesel operated with various feed fuels, the aromatic molecular composition could be unraveled. The type of feed fuel substantially affected the observed chemical profile. Combustion of the diesel revealed a low complex profile dominated by the PAH core compounds. However, expensive diesel fuel is solely being used for testing or domestic shipping. For noncompliant HFO, the impact of the wet scrubber on the gas phase was found to be insignificant. The primary HFO emissions resulted in the

highest and most complex response for the CHS-class. In contrast, for the VLSFO, an increased proportion of species with higher DBE was found. Thus, the VLSFO, containing large amounts of cycle oil, a cheap petroleum refining byproduct, can legally be applied but causes a substantial release of larger PAHs. These compounds are known for their strong environmental and health effects. Conclusively, legislative measures might need to consider further chemical criteria beyond bulk properties, such as FSC.

Future studies will investigate the incomplete combustion products of the thermal degradation of lignocellulosic biomass (log wood stove or ambient wildfire events) or industrial processes, such as coffee or nut roasting. The high-resolution performance and charge capacity of the Orbitrap mass analyzer persuade the application of other light sources, broadening the accessible functionalities, such as laser or lamp VUV light sources for single photon ionization.

## ASSOCIATED CONTENT

# Supporting Information

The Supporting Information is available free of charge at https://pubs.acs.org/doi/10.1021/acs.analchem.2c03972.

Table with estimated limits of detection for standard gas mixture compounds (Table S1); on-site photography and scheme of the setup (Figure S1); exemplary mass spectrum of the gas standard (Figure S2); error histogram for the elemental composition attribution of the engine start-up (diesel  $\rightarrow$  HFO) (Figure S3); total ion current for engine launch (diesel → HFO) (Figure S4); histograms of data shown in Figure 2c,d (Figure S5); visualization of the ratio of the highest to the lowest abundance peak-picked signal and isotopic fine structure profile of C<sub>16</sub>H<sub>10</sub> (Figure S6); time-resolved visualization of the fine isotopic abundance deviations (Figure S7); scenario for identification of unknown species via isotopic ratios (Figure S8); DBE distribution from the averaged HFO spectra over 5 min (Figure S9); mass spectra for various fuels (diesel, HFO, HFO after scrubber, VLSFO) are displayed in the mass range of 0 to 500 m/z averaged over 5 min (Figure S10); compound class distribution of the diesel, HFO (with/ without wet scrubber) and VLSFO emissions (Figures S11-S14); Kendrick mass defect plots (CH2) for the diesel, HFO (with/without wet scrubber) and VLSFO emissions (Figure S15); extracted time-resolved traces for the CH- and CHO-class and  $C_{16}H_{10}O_1$  (DBE 10) and  $C_{15}H_{10}S_1$  (DBE 11) (diesel  $\rightarrow$  HFO, and diesel  $\rightarrow$ VLSFO) (Figure S16) (PDF)

# AUTHOR INFORMATION

# **Corresponding Author**

Christopher P. Rüger — Joint Mass Spectrometry Centre (JMSC)/Chair of Analytical Chemistry, University of Rostock, 18059 Rostock, Germany; Department Life, Light & Matter (LLM), University of Rostock, 18059 Rostock, Germany; orcid.org/0000-0001-9634-9239; Email: christopher.rueger@uni-rostock

# Authors

Paul Kösling – Joint Mass Spectrometry Centre (JMSC)/ Chair of Analytical Chemistry, University of Rostock, 18059 Rostock, Germany; Department Life, Light & Matter (LLM), University of Rostock, 18059 Rostock, Germany; Faculty for Mechanical Engineering, Institute of Chemistry and Environmental Engineering, University of the Bundeswehr Munich, 85577 Neubiberg, Germany

Julian Schade — Joint Mass Spectrometry Centre (JMSC)/ Chair of Analytical Chemistry, University of Rostock, 18059 Rostock, Germany; Department Life, Light & Matter (LLM), University of Rostock, 18059 Rostock, Germany; Faculty for Mechanical Engineering, Institute of Chemistry and Environmental Engineering, University of the Bundeswehr Munich, 85577 Neubiberg, Germany

Sven Ehlert — Photonion GmbH, 19061 Schwerin, Germany Uwe Etzien — Chair of Piston Machines and Internal Combustion Engines, University of Rostock, 18059 Rostock, Germany

Anton N. Kozhinov – Spectroswiss, 1015 Lausanne, Switzerland

Yury O. Tsybin — Spectroswiss, 1015 Lausanne, Switzerland; orcid.org/0000-0001-7533-0774

Martin Rigler – Aerosol d.o.o., SI-1000 Ljubljana, Slovenia Thomas Adam – Faculty for Mechanical Engineering, Institute of Chemistry and Environmental Engineering, University of the Bundeswehr Munich, 85577 Neubiberg, Germany

Andreas Walte - Photonion GmbH, 19061 Schwerin, Germany

Bert Buchholz – Chair of Piston Machines and Internal Combustion Engines, University of Rostock, 18059 Rostock, Germany

Ralf Zimmermann — Joint Mass Spectrometry Centre (JMSC)/Chair of Analytical Chemistry, University of Rostock, 18059 Rostock, Germany; Department Life, Light & Matter (LLM), University of Rostock, 18059 Rostock, Germany; Joint Mass Spectrometry Centre, Cooperation Group "Comprehensive Molecular Analytics", Helmholtz Zentrum Muenchen, D-85764 Neuherberg, Germany

Complete contact information is available at: https://pubs.acs.org/10.1021/acs.analchem.2c03972

## Notes

The authors declare no competing financial interest.

## ACKNOWLEDGMENTS

This work is financed and supported by the EUROSTARS project E! 12083 "AerOrbi". Support by the Helmholtz International Lab. aeroHEALTH (www.aerohealth.eu) is gratefully acknowledged. The authors thank the Interdisciplinary Faculty, Department Life, Light, and Matter of the University of Rostock for providing laboratory space and infrastructure. This work was supported by the Federal Ministry for Economic Affairs and Climate Action by the project SAARUS (grant number 03SX483D) and by dtec.bw-Digitalization and Technology Research Center of the Bundeswehr (project "LUKAS and MORE"). The authors thank Thermo Fisher Scientific for support, especially Tobias Wörner, Kyle Fort, and Alexander Makarov.

# REFERENCES

- (1) Kinney, P. L. Curr. Environ. Health Rep. 2018, 5, 179-186.
- (2) Corbett, J. J.; Winebrake, J. J.; Green, E. H.; Kasibhatla, P.; Eyring, V.; Lauer, A. *Environ. Sci. Technol.* **2007**, *41*, 8512–8518.
- (3) In Review of Maritime Transport, United Nations Conference on Trade and Development; United Nations: New York, Geneva, 2017.

- (4) Blasco, J.; Durán-Grados, V.; Hampel, M.; Moreno-Gutiérrez, J. Environ. Int. **2014**, *66*, 44–47.
- (5) Mueller, L.; Jakobi, G.; Czech, H.; Stengel, B.; Orasche, J.; Arteaga-Salas, J. M.; Karg, E.; Elsasser, M.; Sippula, O.; Streibel, T.; Slowik, J. G.; Prevot, A. S.; Jokiniemi, J.; Rabe, R.; Harndorf, H.; Michalke, B.; Schnelle-Kreis, J.; Zimmermann, R. Appl. Energy 2015, 155, 204–217.
- (6) Sippula, O.; Stengel, B.; Sklorz, M.; Streibel, T.; Rabe, R.; Orasche, J.; Lintelmann, J.; Michalke, B.; Abbaszade, G.; Radischat, C.; Gröger, T.; Schnelle-Kreis, J.; Harndorf, H.; Zimmermann, R. *Environ. Sci. Technol.* **2014**, 48, 11721–11729.
- (7) Streibel, T.; Schnelle-Kreis, J.; Czech, H.; Harndorf, H.; Jakobi, G.; Jokiniemi, J.; Karg, E.; Lintelmann, J.; Matuschek, G.; Michalke, B.; Müller, L.; Orasche, J.; Passig, J.; Radischat, C.; Rabe, R.; Reda, A.; Rüger, C.; Schwemer, T.; Sippula, O.; Stengel, B.; Sklorz, M.; Torvela, T.; Weggler, B.; Zimmermann, R. *Environ. Sci. Pollut. Res.* **2017**, *24*, 10976–10991.
- (8) Czech, H.; Sippula, O.; Kortelainen, M.; Tissari, J.; Radischat, C.; Passig, J.; Streibel, T.; Jokiniemi, J.; Zimmermann, R. Fuel **2016**, 177, 334–342.
- (9) Dallmann, T. R.; Onasch, T. B.; Kirchstetter, T. W.; Worton, D. R.; Fortner, E. C.; Herndon, S. C.; Wood, E. C.; Franklin, J. P.; Worsnop, D. R.; Goldstein, A. H.; Harley, R. A. *Atmos. Chem. Phys.* **2014**, *14*, 7585–7599.
- (10) Pant, P.; Harrison, R. M. Atmos. Environ. 2013, 77, 78-97.
- (11) Canagaratna, M. R.; Massoli, P.; Browne, E. C.; Franklin, J. P.; Wilson, K. R.; Onasch, T. B.; Kirchstetter, T. W.; Fortner, E. C.; Kolb, C. E.; Jayne, J. T.; Kroll, J. H.; Worsnop, D. R. J. Phys. Chem. A 2015, 119, 4589–4599.
- (12) Rivellini, L.-H.; Adam, M. G.; Kasthuriarachchi, N.; Lee, A. K. Y. Atmos. Chem. Phys. **2020**, 20, 5977-5993.
- (13) Lee, C. P.; Riva, M.; Wang, D.; Tomaz, S.; Li, D.; Perrier, S.; Slowik, J. G.; Bourgain, F.; Schmale, J.; Prevot, A. S. H.; Baltensperger, U.; George, C.; El Haddad, I. *Environ. Sci. Technol.* 2020, 54, 3871–3880.
- (14) Schade, J.; Passig, J.; Irsig, R.; Ehlert, S.; Sklorz, M.; Adam, T.; Li, C.; Rudich, Y.; Zimmermann, R. *Anal. Chem.* **2019**, *91*, 10282–10288.
- (15) Passig, J.; Schade, J.; Irsig, R.; Kröger-Badge, T.; Czech, H.; Adam, T.; Fallgren, H.; Moldanova, J.; Sklorz, M.; Streibel, T.; Zimmermann, R. Atmos. Chem. Phys. 2022, 22, 1495–1514.
- (16) Passig, J.; Schade, J.; Irsig, R.; Li, L.; Li, X.; Zhou, Z.; Adam, T.; Zimmermann, R. *Atmos. Meas. Tech.* **2021**, *14*, 4171–4185.
- (17) Oeder, S.; Kanashova, T.; Sippula, O.; Sapcariu, S. C.; Streibel, T.; Arteaga-Salas, J. M.; Passig, J.; Dilger, M.; Paur, H.-R.; Schlager, C.; Mülhopt, S.; Diabaté, S.; Weiss, C.; Stengel, B.; Rabe, R.; Harndorf, H.; Torvela, T.; Jokiniemi, J. K.; Hirvonen, M.-R.; Schmidt-Weber, C.; Traidl-Hoffmann, C.; BéruBé, K. A.; Wlodarczyk, A. J.; Prytherch, Z.; Michalke, B.; Krebs, T.; Prévôt, A. S. H.; Kelbg, M.; Tiggesbäumker, J.; Karg, E.; Jakobi, G.; Scholtes, S.; Schnelle-Kreis, J.; Lintelmann, J.; Matuschek, G.; Sklorz, M.; Klingbeil, S.; Orasche, J.; Richthammer, P.; Müller, L.; Elsasser, M.; Reda, A.; Gröger, T.; Weggler, B.; Schwemer, T.; Czech, H.; Rüger, C. P.; Abbaszade, G.; Radischat, C.; Hiller, K.; Buters, J. T. M.; Dittmar, G.; Zimmermann, R. PLoS One 2015, 10, No. e0126536.
- (18) Kleeblatt, J.; Stengel, B.; Radischat, C.; Passig, J.; Streibel, T.; Sippula, O.; Rabe, R.; Harndorf, H.; Zimmermann, R. *Anal. Methods* **2015**, *7*, 3608–3617.
- (19) Reda, A. A.; Schnelle-Kreis, J.; Orasche, J.; Abbaszade, G.; Lintelmann, J.; Arteaga-Salas, J. M.; Stengel, B.; Rabe, R.; Harndorf, H.; Sippula, O.; Streibel, T.; Zimmermann, R. *Atmos. Environ.* **2015**, *112*, 370–380.
- (20) Czech, H.; Heide, J.; Ehlert, S.; Koziorowski, T.; Zimmermann, R. Foods 2020, 9, 627.
- (21) Dorfner, R.; Ferge, T.; Yeretzian, C.; Kettrup, A.; Zimmermann, R. *Anal. Chem.* **2004**, *76*, 1386–1402.
- (22) Elsasser, M.; Busch, C.; Orasche, J.; Schön, C.; Hartmann, H.; Schnelle-Kreis, J.; Zimmermann, R. *Energy Fuels* **2013**, *27*, 4959–4968.

- (23) Radischat, C.; Sippula, O.; Stengel, B.; Klingbeil, S.; Sklorz, M.; Rabe, R.; Streibel, T.; Harndorf, H.; Zimmermann, R. *Anal. Bioanal. Chem.* **2015**, 407, 5939–5951.
- (24) Idowu, O.; Semple, K. T.; Ramadass, K.; O'Connor, W.; Hansbro, P.; Thavamani, P. *Environ. Int.* **2019**, *123*, 543–557.
- (25) Kösling, P.; Rüger, C. P.; Schade, J.; Fort, K. L.; Ehlert, S.; Irsig, R.; Kozhinov, A. N.; Nagornov, K. O.; Makarov, A.; Rigler, M.; Tsybin, Y. O.; Walte, A.; Zimmermann, R. *Anal. Chem.* **2021**, 93, 9418–9427.
- (26) Mühlberger, F.; Hafner, K.; Kaesdorf, S.; Ferge, T.; Zimmermann, R. Anal. Chem. 2004, 76, 6753-6764.
- (27) Wu, D.; Li, Q.; Ding, X.; Sun, J.; Li, D.; Fu, H.; Teich, M.; Ye, X.; Chen, J. *Environ. Sci. Technol.* **2018**, *52*, 12943–12951.
- (28) Lunde Hermansson, A.; Hassellöv, I.-M.; Moldanová, J.; Ytreberg, E. Trans. Res. Part D: Trans. Environ. 2021, 97, No. 102912.
- (29) Tembreull, R.; Sin, C. H.; Li, P.; Pang, H. M.; Lubman, D. M. Anal. Chem. 1985, 57, 1186–1192.
- (30) Zimmermann, R.; Boesl, U.; Weickhardt, C.; Lenoir, D.; Schramm, K.-W.; Kettrup, A.; Schlag, E. W. Chemosphere 1994, 29, 1877–1888.
- (31) de Oliveira Galvão, M. F.; de Oliveira Alves, N.; Ferreira, P. A.; Caumo, S.; de Castro Vasconcellos, P.; Artaxo, P.; de Souza Hacon, S.; Roubicek, D. A.; de Medeiros, S. R. *Environ. Pollut.* **2018**, 233, 960–970.
- (32) Clergé, A.; Le Goff, J.; Lopez, C.; Ledauphin, J.; Delépée, R. Crit. Rev. Toxicol. 2019, 49, 302–328.
- (33) Walgraeve, C.; Demeestere, K.; Dewulf, J.; Zimmermann, R.; van Langenhove, H. Atmos. Environ. 2010, 44, 1831–1846.
- (34) Streibel, T.; Zimmermann, R. Annu. Rev. Anal. Chem. 2014, 7, 361–381.
- (35) Valavanidis, A.; Vlachogianni, T.; Fiotakis, K.; Loridas, S. Int. J. Environ. Res. Public Health 2013, 10, 3886–3907.
- (36) Käfer, U.; Gröger, T.; Rohbogner, C. J.; Struckmeier, D.; Saraji-Bozorgzad, M. R.; Wilharm, T.; Zimmermann, R. *Energy Fuels* **2019**, 33, 10745–10755.
- (37) Czech, H.; Schnelle-Kreis, J.; Streibel, T.; Zimmermann, R. Atmos. Environ. 2017, 163, 190–191.
- (38) Heide, J.; Ehlert, S.; Koziorowski, T.; Rüger, C. P.; Walte, A.; Zimmermann, R. *Analyst* **2022**, *147*, 3662–3674.
- (39) Kanashova, T.; Popp, O.; Orasche, J.; Karg, E.; Harndorf, H.; Stengel, B.; Sklorz, M.; Streibel, T.; Zimmermann, R.; Dittmar, G. Anal. Bioanal. Chem. 2015, 407, 5965–5976.
- (40) Sapcariu, S. C.; Kanashova, T.; Dilger, M.; Diabaté, S.; Oeder, S.; Passig, J.; Radischat, C.; Buters, J.; Sippula, O.; Streibel, T.; Paur, H.-R.; Schlager, C.; Mülhopt, S.; Stengel, B.; Rabe, R.; Harndorf, H.; Krebs, T.; Karg, E.; Gröger, T.; Weiss, C.; Dittmar, G.; Hiller, K.; Zimmermann, R. *PLoS One* **2016**, *11*, No. e0157964.